On the applicability of single-line equivalents on optimal operation of modern unbalanced distribution networks

Serna-Suárez, I. D.; Morales-España, G.; de Weerdt, M.; Carrillo-Caicedo, G.; Ordóñez-Plata, G.; Quiroga, O. A.

DOI
10.1016/j.epsr.2023.109699

Publication date
2023

Document Version
Final published version

Published in
Electric Power Systems Research

Electric Power Systems Research 223 (2023) 109699

Contents lists available at ScienceDirect

Electric Power Systems Research

journal homepage: www.elsevier.com/locate/epsr

On the applicability of single-line equivalents on optimal operation of modern unbalanced distribution networks ☆

I.D. Serna-Suárez [a,*], G. Morales-España [b], M. de Weerdt [c], G. Carrillo-Caicedo [a], G. Ordóñez-Plata [a], O.A. Quiroga [a]

[a] Escuela de Ingenierías Eléctrica, Electrónica y de Telecomunicaciones, Universidad Industrial de Santander, Colombia
[b] Energy Transition Studies Department, Netherlands Organization for Applied Scientific Research (TNO), The Netherlands
[c] Faculty of Electrical Engineering, Mathematics and Computer Sciences, Delft University of Technology, The Netherlands

ARTICLE INFO

Keywords:
Distributed Energy Resource (DER) scheduling
Optimal power flow
Power distribution networks
Renewable energy
Storage systems

ABSTRACT

The integration of Distributed Energy Resources (DERs) in distribution networks comes with challenges, like power quality concerns, but also opens up new opportunities, e.g., DERs can offer competitive energy prices for final users by leveraging time arbitrage. A suitable method to fully exploit such opportunities is to compute the optimal DER schedule, either with a full three-phase network model or a more computationally efficient single-line equivalent. This paper presents under which conditions a single-line equivalent can and cannot be used to properly represent a modern and unbalanced power distribution network able to dispatch high levels of DER integration optimally. Results show that single-line equivalents might be helpful when the problem objective function limits counterflows, for example, when minimizing active power losses. Moreover, single-line equivalents might be helpful for low levels of DER integration. However, enabling single-line equivalents results in a lower hosting capacity for high levels of DER integration.

1. Introduction

The last years have seen an enormous increase in the number of solar photovoltaic systems (PV), storage and electric vehicle charging across all locations in distribution systems [1,2]. At many places this has led to issues regarding congestion and voltage regulation [3,4]. Integrating such Distributed Energy Resources (DERs) into power distribution networks, however, also comes with several opportunities to make this kind of system more dynamic. For example, an independent Distribution Network Operator (DNO) could use a combination of DERs to improve voltage quality, reduce the network losses [5,6], and a retailer with several DERs may use them to provide ancillary services or to make some profit by taking advantage of daily energy price variations [6–8]. The latter has motivated the appearance of the prosumer, demand response, and virtual power plant concepts in distribution networks [8,9]. Actually, entrepreneurs from all over the world have seen here a prolific space to grow, by giving independence to the PV owners through storage and efficient energy management strategies [10]; by using all the PV and storage systems to form a virtual power plant able to support the power system operation [11]; or by using a shared storage model to increase PV integration and reduce final user energy costs [12,13].

This is a trend that will only become more ubiquitous in the near future, thus, increasing the integration levels of PV systems and storage systems even further. In turn, these high levels of non-dispatchable renewable sources may increase system losses on peak production [5,14]. Furthermore, it may increase the voltage unbalance [15], and even may be added to the existing unbalance due to one-phase loads [16]. Therefore, proper modeling of three-phase elements is key to enhancing the model applicability [17,18].

1.1. Literature review

From the above, one may conclude that there is a consensus about the importance of a full 3-phase Alternating Current Optimal Power Flow (3ϕ-ACOPF) [19], moreover, with recent advances in mathematical programming and data science, the limits on what is possible to compute are being expanded quickly.

For example, linearizations like the ones presented in [20] and [21] show that curve fitting around an operation point of the proper

☆ This research has been funded by the "Universidad Industrial de Santander" (Santander, Colombia) through the research project VIE-UIS 2695 and the 528 COLCIENCIAS-COLFUTURO (Colombia) scholarship programme.

* Corresponding author.
E-mail address: idsersua@uis.edu.co (I.D. Serna-Suárez).

https://doi.org/10.1016/j.epsr.2023.109699
Received 13 April 2023; Received in revised form 22 June 2023; Accepted 8 July 2023
Available online 19 July 2023

List of Symbols

Sets

$\mathcal{T}$	Set of time periods, where $\|\mathcal{T}\| = \tau$.
$\mathcal{N}$	Set of network nodes, where $\|\mathcal{N}\| = N$.
$\mathcal{R}$	Set of network branches, where $\|\mathcal{R}\| = R$.
$\mathcal{G}$	Set of elements able to inject power into the network, where $\|\mathcal{G}\| = G$.
$\mathcal{D}$	Set of loads, where $\|\mathcal{D}\| = D$.
$\boldsymbol{\Phi}$	Set of network phase-to-ground connections.
$\mathcal{F}$	Set of network phase-to-phase connections.

Indices

t	Time period, $t \in \mathcal{T}$.
n, m	Node, $n, m \in \mathcal{N}$.
(n, m)	Branch for which the n node is the "from/sending" node and the m node is the "to/receiving" node, $n, m \in \mathcal{N}$.
$r(m, n)$	Branch for which the m node is the "from/sending" node and the n node is the "to/receiving" node, $r \in \mathcal{R}, r = \{m, n\}$ and $m, n \in \mathcal{N}$.
ϕ, φ	Phase-to-ground connection/element, ϕ, $\varphi \in \boldsymbol{\Phi}$.
$\phi\varphi$	Phase-to-phase connection/element, $\phi\varphi \in \mathcal{F}$ and ϕ, $\varphi \in \boldsymbol{\Phi}$.
g	Generator, $g \in \mathcal{G}$.
d	Demand, $d \in D$.
S	Constant apparent power component of a demand.
I	Constant current component of a demand.
Z	Constant impedance component of a demand.
Δ	Delta branch phase-to-phase connection.
$\curlyvee$	Wye load.
$\vartriangle$	Delta load.

Parameters

$P_g^{\text{av.},\phi}$	Available PV energy.
$\Theta_g^{\max.}$	Maximum angle difference between same phase current and voltage phasors.
ϵ_{in}	Storage system power injection efficiency.
ϵ_{ou}	Storage system power withdraw efficiency.
E_g	Maximum storage energy capacity.
Δt	Period duration (1 h).
y_n^{ϕ}	Shunt admittance at phase ϕ of node n.
$y_{r(n,m)}^{\phi\varphi,\text{from}}$	Component $\phi\varphi$ of the series branch admittance matrix of line r as seen from the sending end (node n) of the line.
$y_{r(n,m)}^{\phi\varphi,\text{to}}$	Component $\phi\varphi$ of the series branch admittance matrix of line r as seen from the receiving end (node m) of the line.
$\tilde{Y}_d$	Constant admittance component of demand d.
$\tilde{I}_d$	Constant current component of demand d.
$\tilde{S}_d$	Constant power component of demand d.
ρ	Regularization factor used to diminish the impact of the time arbitrage over the other objectives.
π	Energy price vector at system header.

Variables

V_x^{ϕ}	Element x applied voltage at phase ϕ, $x \in \mathcal{N} \cup \mathcal{R} \cup \mathcal{G} \cup \mathcal{D}$.
I_x^{ϕ}	Element x injected current at phase ϕ, $x \in \mathcal{N} \cup \mathcal{R} \cup \mathcal{G} \cup \mathcal{D}$.
S_g^{ϕ}	Element g injected apparent power at phase ϕ, $S_g^{\phi} = P_g^{\phi} + jQ_g^{\phi}$.
$\hat{P}_g^{\phi}$	Storage system g injected active power at phase ϕ.
$\check{P}_g^{\phi}$	Storage system g withdrawn active power at phase ϕ.
SOC_g^{ϕ}	Storage system g State of Charge at phase ϕ.
p_g^{ϕ}	Photovoltaic system g curtailed active power at phase ϕ.
F	Objective function (see Section 4.2).

variables might be useful. The former fits the linear combination of the voltage L-infinity and L-one norms to remove the non-linearity introduced by voltage limits; and the latter use a linear polynomial representation of the ZIP load model (assuming constant impedance ("Z"), constant current ("I"), and constant power ("P")) for which parameters are fitted using nominal operation data. In general, as presented in [22], 3ϕ-ACOPF approximations around voltage operation points seem to pose an efficient alternative. This can be further exploited by using fixed-point iterations [23–25] or even lead to a *forced convergent* algorithm [26] which explores the current point neighborhood to come up with a good approximation of the non-linear 3ϕ-ACOPF. All these cases, within their respective simulation conditions, outperform the non-linear model in computation time.

Further, data science can be applied to handle the inherent uncertainty that comes from intermittent DERs, e.g., by constructing an ambiguity set for the probability distribution of the DER outputs [27], thus, improving the cost-effectiveness of the short-term operation when including a closed loop that is able to refresh the variable forecasts given new data. Also, historical or synthetic data can be leveraged with ensemble learning techniques to increase the computational and convergence performance of Semidefinite Programming approaches — which is achieved by fitting the matrix coefficients related to the power balance constraint [28]. On the other hand, Karagiannopoulos et al. [29] use Machine learning Methods to derive an off-line and secure real-time control for DERs.

The main drawback of the studies above is that since the focus is on deriving a proper 3ϕ-ACOPF formulation, no sensitivity analysis or extreme case analysis is done to explore the consequences that such optimal operation point enforcement can have on the network, e.g., on node voltage unbalance. Moreover, when analyzing the impact of DER integration in power distribution systems, most works use one-line equivalents [30] or almost balanced conditions [31]. This opens several questions: Are such almost balanced conditions a consequence of the optimal dispatch or are they inherent to the network? For an inherently unbalanced network, is it possible to find an operation point for which the almost balanced conditions apply? For an inherently almost balanced network, does it remain balanced irrespective of the objective function? When analyzing DER integration by computing the network hosting capacity, is the hosting capacity affected by the objective function or the network unbalance?

Some researchers have studied such consequences under a three-phase model framework, however, they are limited in scope. For example, in [32] the authors explore the effects of the optimal DER dispatch (including PV and storage systems) on the network, but only for a single objective function, leaving open questions about the network behavior with other objectives. On the other hand, Zamzam et al. [33] present a comparison between a one-phase and three-phase OPF, but for a single scenario and without considering system storage. Also, the

focus could be on a single parameter, like in [15], where the voltage unbalance is analyzed for a specific DER combination (PV with reactive compensation, but without storage); or the focus was on the differences against no optimal control, like in [34]. In this respect, Baran et al. [16] explore the differences between a three-phase and a one-phase model for DER sizing, not optimal operation.

1.2. Contributions

The use of single-line equivalents can be helpful in gaining a general understanding of the topology of a distribution network and in facilitating planning, maintenance, and crew routing and dispatch, i.e., single-line equivalents provides a simplified representation of the distribution system that is easy to understand and analyze.

From the previous literature review, it seems clear that modeling only one phase is helpful for power flow analysis of almost balanced distribution networks. As a consequence, although the increasing capability of computers allow us to avoid the single-line equivalent simplification for some traditional problems, the underlying belief is that such simplification introduce an acceptable error for any power distribution system. On the other hand, the single-line equivalent simplification can be fully exploited together with the increasing capability of computers, thus allowing us to solve more demanding problems, e.g., investment problems including storage, sector coupling and uncertainty management with robust/stochastic optimization.

However, single-line equivalents cannot describe the behavior of elements causing a potential unbalance nor the consequences of such an unbalance in the network. In this respect, there is a clear gap in understanding the conditions that induce either the almost balanced or unbalanced state in modern power distribution systems with high integration of renewable energy and storage systems.

Therefore, the main contribution of this paper is to clearly characterize under which conditions a single-line equivalent can and cannot be used to properly represent an unbalanced power distribution network able to dispatch PV and storage systems given a predefined objective function and operational constraints. This is of particular importance given the current decentralization and digitalization trend that modern power distribution networks are going through.

To investigate the conditions when single-line equivalents cannot properly represent an unbalance distribution network, this paper presents a comprehensive study and analysis of 144 simulation cases consisting of all possible combinations of four types of changes: varying the network unbalance; changes of the DER types; changes of the objective function type; and changes of PV installed capacity. All these changes are implemented under the same simulation framework; consequently, questions related to the relevance of reactive compensation and/or electrical storage can also be answered, along with questions about the impacts that 3ϕ-ACOPF impose on the network operation.

1.3. Outline

This paper is organized as follows: Sections 2 to 3, present the nomenclature, system element models and problem definitions; Section 4 describes the implemented cases; later, Section 5 presents all simulation results; the paper ends with some concluding remarks in Section 6.

2. Nomenclature

A sub-index in any set indicates that a specific partition is being made, e.g., for a node $n \in \mathcal{N}$, Φ_n denotes all the phases connected to such node; for a generator $g \in \mathcal{G}$, $\mathcal{G}_{\text{pv}}$ denotes all generators which are Photovoltaic Systems (PV); whereas, for a generator $g \in \mathcal{G}$, $\mathcal{G}_{\text{ss}}$ denotes all generators which are Storage Systems (SS). For a complex number C, its complex conjugate is denoted by $\bar{C}$; $\Re\{C\} = C^{\text{r}}$ and $\Im\{C\} = C^{\text{i}}$ are their real and imaginary parts, respectively; and $|C|$ and $\angle\delta_C$ denote its magnitude and angle δ_C. To keep notation simple, all variables and constants are intended to be column vectors unless the contrary is specified, therefore, each component of a vector is the value of the variable in the corresponding time period, e.g., for $C = [C_1, C_2 \dots C_\tau]$, $C_t \in \mathbb{C}$ is the value at time t. With this in mind, all operations and equations are supposed to be time-component wise, e.g., for two complex vectors A and B, and $T = 2$, $A/B = C$, means $A_1/B_1 = C_1$ and $A_2/B_2 = C_2$. Again, this is true unless the contrary is specified.

3. Problem definition

Table 1 presents the 3ϕ-ACOPF formulation used for each simulation. For all cases and each time period, decision variables are the real and imaginary components of voltages, injected currents and branch currents for each connected phase. On the DER side, the decision variables are the active power curtailed for each PV system and the storage system active power injected into and withdrawn from the network. When including PV reactive compensation, reactive power injected by each PV system for each connected phase is also a decision variable. Also, it is worth noticing the Power Flow Constraints are the set of equations that, when solved simultaneously, give the solution of a three-phase power flow (see Section 3.1) and F depends on the case being analyzed (see Section 4.2).

3.1. Power flow equations

Power flow constraints are summarized in Table 2 for the sake of reference. This formulation is based on the Current Injection Method found in [19,21,35–39], being the main difference the load formulation: In this case, the nominal power and voltage are used to derive the ZIP load parameters, which then are used to directly model the load behavior.

The solution of the three-phase power flow without DERs can be calculated by solving the Power Flow Constraints for a given network topology and the following problem parameters: The voltage angle references of the header node ($\angle\delta_{V_h^{\text{a}}} = 0°$, $\angle\delta_{V_h^{\text{b}}} = -120°$, $\angle\delta_{V_h^{\text{c}}} = 120°$); the voltage profile at the header for a given time window (V_h^{ϕ}); the line admittances ($y_{r(n,m)}^{\phi\varphi,\text{from}}$, $y_{r(n,m)}^{\phi\varphi,\text{to}}$); and the ZIP load parameters ($\tilde{S}_d^{\phi}$, $\tilde{I}_d^{\phi}$, $\tilde{Y}_d^{\phi}$, $\tilde{S}_d^{\Delta}$, $\tilde{I}_d^{\Delta}$, $\tilde{Y}_d^{\Delta}$).

3.2. Objective functions

Four types of objectives functions are considered: active power costs, weighted squared apparent power costs, costs of active power losses and storage arbitrage benefits. All objectives consider that energy is bought at the system header for a given price at each time t given by $\pi_t \in \mathbb{R}_+$, so $\pi \in \mathbb{R}_+^{\tau}$.

Active power costs. Suppose that the DNO wants to minimize the total energy consumption costs at the system header. The active power costs at the system header (f^{p}) are:

$$f^{\text{p}} = \sum_{\phi\in\Phi} \sum_{t\in\mathcal{T}} \pi_t P_{h,t}^{\phi} \tag{29}$$

Weighted squared apparent power costs. Suppose that the DNO wants to minimize active and reactive power imports [40]. Different weights can be given to them, however, to make comparisons with other objectives easier, let us use the same weight for both and use the energy price at the header as such a weight for all power transfers and time periods. Therefore, the weighted square apparent power costs (f^{s}) are:

$$f^{\text{s}} = \sum_{\phi\in\Phi} \sum_{t\in\mathcal{T}} \pi_t \left[\left(P_{h,t}^{\phi} \right)^2 + \left(Q_{h,t}^{\phi} \right)^2 \right] \tag{30}$$

Table 1
Three-phase alternating current optimal power flow.

Objective function		
$\max\{F\}$		
Power flow constraints		
See Table 2		
PV System constraints		
Apparent power	$S_g^\phi = V_n^\phi \bar{I}_g^\phi \; \forall g \in \mathcal{G}_{\text{pv}}, \forall n \in \mathcal{N}_g, \forall \phi \in \boldsymbol{\Phi}_g$	(1)
Power curtailment	$P_g^\phi = P_g^{\text{av.},\phi} - p_g^\phi \; \forall g \in \mathcal{G}_{\text{pv}}, \forall \phi \in \boldsymbol{\Phi}_g$	(2)
Maximum power factor	$\lvert Q_g^\phi \rvert \leq P_g^\phi \tan \Theta_g^{\text{max.}} \; \forall g \in \mathcal{G}_{\text{pv}}, \forall \phi \in \boldsymbol{\Phi}_g$	(3)
Storage system (SS) constraints		
Apparent power	$S_g^\phi = V_n^\phi \bar{I}_g^\phi \; \forall g \in \mathcal{G}_{\text{ss}}, \forall n \in \mathcal{N}_g, \forall \phi \in \boldsymbol{\Phi}_g$	(4)
Power from/to the grid	$P_g^\phi = \hat{P}_g^\phi - \check{P}_g^\phi \; \forall g \in \mathcal{G}_{\text{ss}}, \forall \phi \in \boldsymbol{\Phi}_g$	(5)
Power from/to the Storage System	$\tilde{P}_g^\phi = \hat{P}_g^\phi / \epsilon_{in} - \check{P}_g^\phi \times \epsilon_{ou} \; \forall g \in \mathcal{G}_{\text{ss}}, \forall \phi \in \boldsymbol{\Phi}_g$	(6)
SOC definition	$\tilde{P}_{g,t}^\phi = \left(SOC_{g,t-1}^\phi - SOC_{g,t}^\phi \right) E_g / \Delta t \; \forall g \in \mathcal{G}_{\text{ss}}, \forall \phi \in \boldsymbol{\Phi}_g, \forall t \in \mathcal{T}$	(7)
SOC limits	$SOC_g^{\text{min.}} \leq SOC_g^\phi \leq 1 \; \forall g \in \mathcal{G}_{\text{ss}}, \forall \phi \in \boldsymbol{\Phi}_g$	(8)
SOC final and initial conditions	$SOC_{g,0}^\phi = SOC_{g,\tau}^\phi = SOC_g^{\text{min.}}, \; \forall g \in \mathcal{G}_{\text{ss}}, \forall \phi \in \boldsymbol{\Phi}_g$	(9)
Maximum power export rate	$\hat{P}_g^\phi \leq P_g^{\text{max.}} \times \epsilon_{in} \; \forall g \in \mathcal{G}_{\text{ss}}, \forall \phi \in \boldsymbol{\Phi}_g$	(10)
Maximum power import rate	$\check{P}_g^\phi \leq P_g^{\text{max.}} / \epsilon_{ou} \; \forall g \in \mathcal{G}_{\text{ss}}, \forall \phi \in \boldsymbol{\Phi}_g$	(11)
Voltage constraints		
Voltage magnitude limits	$\lvert V_n^{\text{min}} \rvert^2 \leq \lvert V_n^\phi \rvert^2 \leq \lvert V_n^{\text{max}} \rvert^2 \quad \forall \phi \in \boldsymbol{\Phi}_n, \forall n \in \mathcal{N}$	(12)
Voltage angle reference (phase a)	$\Im\{V_h^{\text{a}}\} = 0$	(13)
Voltage angle reference (phase b)	$\Im\{V_h^{\text{b}}\} = \Re\{V_h^{\text{b}}\} \tan(-2\pi/3)$	(14)
Voltage angle reference (phase c)	$\Im\{V_h^{\text{c}}\} = \Re\{V_h^{\text{c}}\} \tan(-4\pi/3)$	(15)

Table 2
Power flow constraints.

Current balance equations			
Node	$I_n^\phi = \sum_{g \in \mathcal{G}_n} I_g^\phi - \sum_{d \in \mathcal{D}_n} I_d^\phi \quad \phi \in \boldsymbol{\Phi}_n, \forall n \in \mathcal{N}$		(16)
Total demand	$I_d^\phi = I_{\curlyvee d}^\phi + I_{\vartriangle d}^\phi, \quad d \in \mathcal{D}_n, \; \phi \in \boldsymbol{\Phi}_d$		(17)
Network	$I_n^\phi = y_n^\phi V_n^\phi + \sum_{r \in \mathcal{R}_n} I_{(n,m)}^\phi \; \phi \in \boldsymbol{\Phi}_n, \forall n \in \mathcal{N}$		(18)
Line	$I_{(n,m)}^\phi = \sum_{\varphi \in \boldsymbol{\Phi}_n} \left(y_{r(n,m)}^{\phi\varphi,\text{from}} V_n^\varphi + y_{r(n,m)}^{\phi\varphi,\text{to}} V_m^\varphi \right) \; \forall \phi \in \boldsymbol{\Phi}_r, \forall r \in \mathcal{R}$		(19)
Wye demand	$I_{\curlyvee d}^\phi = I_{S\curlyvee d}^\phi + I_{I\curlyvee d}^\phi + I_{Z\curlyvee d}^\phi \; d \in \mathcal{D}_{\curlyvee n}, \; \phi \in \boldsymbol{\Phi}_d$		(20)
Delta demand	$I_{\vartriangle d}^\phi = \sum_{\Delta \in \mathcal{F}_\phi} I_{S\vartriangle d}^\Delta + \sum_{\Delta \in \mathcal{F}_\phi} I_{I\vartriangle d}^\Delta + \sum_{\Delta \in \mathcal{F}_\phi} I_{Z\vartriangle d}^\Delta, \; d \in \mathcal{D}_{\vartriangle n}, \; \phi \in \boldsymbol{\Phi}_d$		(21)
Electrical element definitions			
Header power injection	$S_g^\phi = V_h^\phi \left(I_g^\phi \right)^*$	$g \in \mathcal{G}_h, \; \phi \in \boldsymbol{\Phi}_g$	(22)
Constant power wye load	$\tilde{S}_d^\phi = V_n^\phi \left(I_{S\curlyvee d}^\phi \right)^*$	$n \in \mathcal{N}_{S\curlyvee}, \; d \in \mathcal{D}_{\curlyvee n}, \; \phi \in \boldsymbol{\Phi}_d$	(23)
Constant current wye load	$\tilde{I}_d^\phi = I_{I\curlyvee d}^\phi$	$n \in \mathcal{N}_{I\curlyvee}, \; d \in \mathcal{D}_{\curlyvee n}, \; \phi \in \boldsymbol{\Phi}_d$	(24)
Constant impedance wye load	$I_{Z\curlyvee d}^\phi = \tilde{Y}_d^\phi V_n^\phi$	$n \in \mathcal{N}_{Z\curlyvee}, \; d \in \mathcal{D}_{\curlyvee n}, \; \phi \in \boldsymbol{\Phi}_d$	(25)
Constant power delta load	$\tilde{S}_d^\Delta = V_n^\Delta \left(I_{Sd}^\Delta \right)^*$	$\Delta \in \mathcal{F}, \; n \in \mathcal{N}_{S\vartriangle}, \; d \in \mathcal{D}_{\vartriangle n}$	(26)
Constant current delta load	$\tilde{I}_d^\Delta = I_{Id}^\Delta$	$\Delta \in \mathcal{F}, \; n \in \mathcal{N}_{I\vartriangle}, \; d \in \mathcal{D}_{\vartriangle n}$	(27)
Constant impedance load	$I_{Zd}^\Delta = \tilde{Y}_d^\Delta V_n^\Delta$	$\Delta \in \mathcal{F}, \; n \in \mathcal{N}_{Z\vartriangle}, \; d \in \mathcal{D}_{\vartriangle n}$	(28)

Costs of active power losses. Total losses for each time period in a three-phase power distribution system (P^{LOSS}) can be calculated as:

$$P^{\text{LOSS}} = \sum_{r \in \mathcal{R}} \sum_{\phi \in \boldsymbol{\Phi}_r} P_r^{\text{LOSS},\phi} = \sum_{r \in \mathcal{R}} \sum_{\phi \in \boldsymbol{\Phi}_r} \Re \left\{ V_n^\phi \bar{I}_{(n,m)}^\phi + V_m^\phi \bar{I}_{(m,n)}^\phi \right\} \tag{31}$$

Assuming $I_{(m,n)} \approx -I_{(n,m)}$:

$$P^{\text{LOSS}} = \sum_{r \in \mathcal{R}} \sum_{\phi \in \boldsymbol{\Phi}_r} \Re \left\{ \bar{I}_{(n,m)}^\phi \left(V_n^\phi - V_m^\phi \right) \right\} \tag{32}$$

Then, if the current through the line shunt admittance is much less than the current flowing through the line series impedance, and since $z_{r(n,m)}^{\phi\varphi} = z_{r(n,m)}^{\varphi\phi}$ and with $\Re\left\{ z_{r(n,m)}^{\phi\varphi} \right\} = \text{R}_{r(n,m)}^{\phi\varphi}$ for all connected phases, Eq. (32) can be written as:

$$P^{\text{LOSS}} = \sum_{r \in \mathcal{R}} \left\{ \sum_{\phi,\varphi \in \boldsymbol{\Phi}_r} \text{R}_{r(n,m)}^{\phi\phi} \left| I_{(n,m)} \right|^2 + \sum_{\phi,\varphi \in \{\mathcal{F} \cap \boldsymbol{\Phi}_r\}} \text{R}_{r(n,m)}^{\phi\varphi} \left[\Re \left(I_{(n,m)}^\phi \bar{I}_{(n,m)}^\varphi \right) \right] \right\} \tag{33}$$

So, ignoring the coupling effects:

$$P^{\text{LOSS}} = \sum_{r \in \mathcal{R}} \sum_{\phi \in \boldsymbol{\Phi}_r} \left\{ \text{R}_{r(n,m)}^{\phi\phi} \left| I_{(m,n)} \right|^2 \right\} \tag{34}$$

Eq. (31) gives the exact value for losses, while (33) gives a good estimation for the network losses. On the other hand, (34) have been reported in the literature [32,41,42] as a surrogate of the total losses equation. In general, total losses are defined as $L_T = \sum_{t \in \mathcal{T}} P_t^{\text{LOSS}}$. Thus, total costs of active power losses (f^{LOSS}) can be defined as:

$$f^{\text{LOSS}} = \sum_{t \in \mathcal{T}} \pi_t P_t^{\text{LOSS}} \tag{35}$$

Storage arbitrage benefits. As reported in [43], by assuring that the round-trip efficiency of the storage system is less than one (i.e., $\epsilon_{in}\epsilon_{ou} < 1$), given that prices are always positive ($\pi \in \mathbb{R}_+^\tau$), and assuming that power injections are meant to be maximized and power withdrawals are meant to be minimized, one can model the storage device behavior without discrete variables if the following objective function is used:

$$f^{\text{SS}} = \frac{1}{\rho} \sum_{g \in \mathcal{G}_{\text{ss}}} \sum_{\phi \in \boldsymbol{\Phi}_g} \sum_{t \in \mathcal{T}} \pi_t \left[\hat{P}_{g,t}^\phi - \check{P}_{g,t}^\phi \right] \tag{36}$$

Where f^{ss} are the total arbitrage benefits that are captured by the electrical storage systems in the network and ρ is a scaling factor used to diminish the impact of the time arbitrage over the other objectives. The choice of ρ when combining objective functions is very important: If ρ is too large, f^{ss} will lose importance in the optimization, and so the storage injections. As a consequence, $\hat{P}_g^{\phi}$ and $\check{P}_g^{\phi}$ might have values different to zero on the same time period, i.e., the ES will be charging and discharging power at the same time, which is physically impossible [43]. Furthermore, the ρ parameter can be used to adjust what it would be considered as "zero" when charging or discharging energy. Hence, depending on the value of ρ a zero $\hat{P}_g^{\phi}$ or $\check{P}_g^{\phi}$ can vary from 1×10^{-1} to 1×10^{-7}.

4. Test cases

On this section we introduce the four dimensions of network properties we considered to establish the accuracy of single-line equivalent models. These variants define in total 144 different study cases. Section 4.1 describes the circuit types. This change is to see how useful a balanced model (thus, a one-line equivalent) is when analyzing unbalanced systems. Section 4.2 presents the objectives used. By varying the objective function and analyzing their effects on the network, one can arrive at criteria for choosing the objective according to the desired outcome. Section 4.3 details the DER configuration types. Changing the DER type helps to see if PV reactive compensation and storage are complementary measures for the network's reactive and active power control. All these changes are also tested for three irradiance levels, described in Section 4.4.

Finally, the system parameters presented in Section 4.5 are computed for each case. All cases were implemented on a laptop computer with an Intel Core i7 processor at 2.4 GHz with 6 GB of RAM. The presented models were implemented in GAMS using IPOPT solver because of its computational performance, and to avoid fine tuning solver parameters between cases.

4.1. Circuits

Three test systems are studied, all of them based on the IEEE 34 node test feeder [44], and with the following modifications:

(1, CPLT): This is the complete circuit (see Fig. 1), the only modifications being that the regulator taps are set as presented in Table 3.

(2, UNBL): This is the circuit with only unbalanced load. Regulator tap is the same than CPLT case, and all non-three-phase branches were removed; all loads that were on such branches were moved to the nearest three-phase node. This circuit helps to differentiate the error induced by ignoring system unbalance, and the error induced by ignoring non-three-phase laterals.

(3, BALN): This is the equivalent balanced circuit; thus, answers with this circuit are the same as those obtained with a single-line equivalent. Regulator taps are the same for each phase, and were set to 7 and 10 for regulators at branches 814–850 and 852–832, respectively. Also, all non-three-phase branches are treated as in the UNBL circuit. Besides, all lines are transposed and non-balanced loads/DERs were transformed to a balanced three-phase equivalent.

4.2. Objectives

Four objectives are studied: (1, PCOSTS) Minimizing total active power import costs at the header, i.e., $F = f^{ss} - f^{p}$; (2, SCOSTS) Minimizing total weighted apparent power import costs at the header, i.e., $F = f^{ss} - f^{s}$; (3, LOSS) Minimizing the active power losses considering line coupling effects, i.e., $F = f^{ss} - f^{LOSS}$ using (33); (4, SLF-LOSS) Minimizing the active power losses without line coupling effects, i.e., $F = f^{ss} - f^{LOSS}$ using (34). In all cases f^{ss} equals zero if there is no storage; for cases with storage f^{ss} is at least three orders of magnitude lower than the other objective. Moreover, ρ is further adjusted so $\hat{P}_g^{\phi}$ and $\check{P}_g^{\phi}$ are at least 1×10^{-5} when charging and discharging, respectively.

Table 3
Test feeder parameters for the CPLT circuit.

DER nodes	Voltage limits	Regulators (from-to nodes)		
		a	b	c
810-b, 820-a, 826-b, 864-a, 890, 848, 840, 838-b, 856-b, 844, 830, 802, 832	0.90 to 1.05 Vp.u.	814–850		
		14	7	7
		852–832		
		12	10	11
Storage system parameters				
$\epsilon_{in} = 0.9,\ \epsilon_{ou} = 0.8,\ SOC_{min} = 0.1,\ SOC_{max} = 1$				

DERs with unspecified phases are connected to all three phases, i.e., they are connected to phase a, b and c.

4.3. DER models

Four DER models are studied, all including PV generation with curtailment at nodes presented in Table 3: (1, B) This is the Base case, i.e., PV with curtailment ; (2, Q) Same as case (1), but with reactive compensation on each PV system — minimum power factor equal to 0.9; (3, SS) Same as case (1), but with storage; and (4, SS-Q) Same as case (2), but with storage. Storage and/or reactive compensation are/is placed at nodes with PV generation.

4.4. PV levels

Solar level is here defined as the ratio between the total available irradiance and the total active power injections at the system header without DERs. This is similar to the ratio between PV installed capacity and the header substation rated capacity presented in [42]. Three PV integration levels are studied: (1, max.) Full irradiance, which has a 129% of PV integration; (2, med.) 3/5 of the total irradiance, which has a 77% of PV integration; and (3, min.) 1/5 of the total irradiance, which corresponds to 26% of PV integration. The last two integrations are typical values [32,33,39,42], while the former is used to test the impacts of very high integrations on the distribution network, a needed feature of future distribution networks given the rapid increase of installed solar capacity [33,39,42].

4.5. System parameter calculations

For each case, apart from the objective functions, apparent power injected by all PV systems is calculated as:

$$S_T^{pv} = \Sigma^{tot.}\left(S_g,\ g \in \mathcal{G}_{pv}\right) = \sum_{g \in \mathcal{G}_{pv}} \sum_{\phi \in \Phi_g} \imath^T S_g^{\phi}$$

Being $\imath$ a column vector of ones, so $\imath^T S_g^{\phi} = \sum_{t \in \mathcal{T}} S_{g,t}^{\phi}$. Other system parameters are as well calculated: Total curtailed PV active power ($p_T = \Sigma^{tot.}\left(p_g,\ \forall g \in \mathcal{G}_{pv}\right)$), total injected storage energy ($P_T^{\wedge} = \Sigma^{tot.}\left(\hat{P}_g^{\phi},\ \forall g \in \mathcal{G}_{ss}\right)$), total withdrawn storage energy ($P_T^{\vee} = \Sigma^{tot.}\left(\check{P}_g^{\phi},\ \forall g \in \mathcal{G}_{ss}\right)$), total apparent power at the system header ($S_T^{h} = P_T^{h} + jQ_T^{h} = \Sigma^{tot.}\left(S_g,\ g \in \{h\}\right)$) and the negative and zero sequence Voltage Unbalance Factor (VUF) for all three-phase nodes. For example, the negative sequence VUF for the node n is defined as:

$$VUF_n^{(-)} = \frac{|V_n^{(-)}|}{|V_n^{(+)}|} = \frac{|V_n^{a} + aV_n^{b} + a^2V_n^{c}|}{|V_n^{a} + a^2V_n^{b} + aV_n^{c}|}$$

Where $a = 1\angle -120°$.

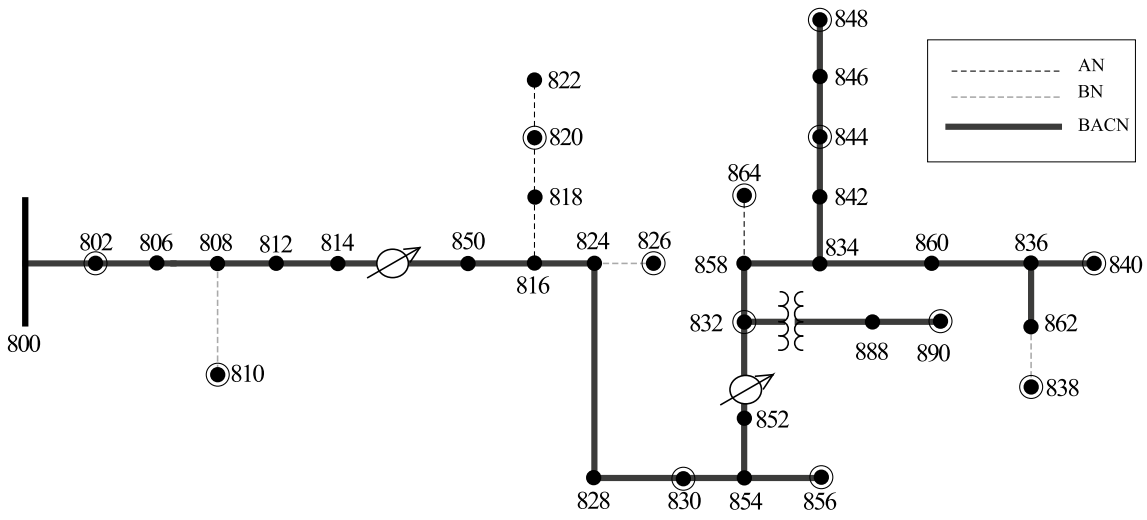

Fig. 1. IEEE 34 node test feeder [44]. Circled nodes have DER injections.

5. Results

This section summarizes the results of the 144 different study cases following the four dimensions of network properties described in Section 4. Results due to changes in the circuit are presented in Section 5.1, changes in the objective functions are presented in Section 5.2, and changes in the DER configuration types are presented in Section 5.3. As pointed out in Section 4, changes in irradiance are included within each of the three other changes; therefore, each analysis below considers variations in two dimensions.

5.1. Circuit variations

With PCOSTS as objective, the differences between CPLT and BALN circuits become larger as the PV installed capacity increases. This is due to differences in the moments where active power injections take place, as for a low difference in the total energy injected by storage systems there is a big difference in the total time arbitrage benefits (up to 28% more benefits are captured for maximum irradiance, see Table 4.a, max irradiance rows of f^{SS}columns).

Besides, note that BALN circuit have lower curtailed active power (up to 80.1% less for medium irradiance, see Table 4.a, medium irradiance rows of p_T columns) and lower PV reactive consumption (up to 176% less for medium irradiance, see Table 4.a, medium irradiance rows of Q_T^{PV} columns), causing lower total active power injections at system header (up to 279% less for maximum irradiance, see Table 4.a, maximum irradiance rows of P_T^h columns). So, when using power injections from the BALN circuit in the CPLT circuit, one might expect voltage violations to occur.

In general, the errors seen in BALN with respect to the CPLT case when using PCOSTS objective are due to the higher availability of active power in the BALN system, which in turn increases reversed active power flows. This is corroborated for the minimum PV level case, where the power curtailment is zero for all cases, and the available irradiance is not enough to cause significant reversed flows. There, results from CPLT and BALN circuits and from CPLT and UNBL circuits are closer. Furthermore, these results are very similar to those obtained using SCOSTS and LOSS objectives.

When the objective function causes a reduction in active power losses, like for the case of SCOSTS and LOSS objectives, the errors in curtailed power are the smaller among all cases (see Table 4.b). Moreover, these errors are smaller when trying to dispatch storage at ending nodes (see Fig. 2). Hence, because losses may increase due to the higher availability of active power in the BALN circuit, the PV available power is curtailed to reduce reversed flows if needed.

Since the lowest network losses are those appearing with the BALN circuit, it makes sense that, when trying to minimize active losses costs in an unbalanced system, the solutions are as balanced as possible. In contrast, although BALN circuit has the lowest values of active power costs at system header, the more unbalance have the CPLT circuit, the lower are the active power costs. This is mainly because it is more effective to improve PCOSTS objective function by maximizing the negative entries of P_h than by reducing system unbalance.

5.2. Objective variations

Three-phase power flow results are presented in Table 5 along with the three-phase optimal power flow without and with DERs, the latter being for maximum PV integration and SS-Q DER case. There, PCOSTS gives the lower costs and the highest system losses among studied cases. On the other hand, LOSS gives the lower system losses among studied cases.

Note that for the PCOSTS objective, lower costs are achieved by increasing reactive power consumption. This is because higher active power injections tend to increase the system voltage magnitude, therefore, consumption of reactive power must be increased to maintain voltages within the operational limits. Overall, for high and medium PV integration, PV reactive power injections have a lagging power factor when using the PCOSTS objective, whereas for all other objectives, PV reactive power injections have a leading power factor. For minimum PV integration, all cases have a leading power factor.

Differences between LOSS and SLF-LOSS are usually less than or equal to 1% in each of the monitored parameters, indicating that mutual impedance have a small effect when minimizing active power losses. SCOSTS and LOSS objectives are also very similar; however, their differences range from 2% to 6%. Besides, since the current magnitude depends on the active and reactive power, minimizing the cost of line active power losses results in the lowest reactive power flows among cases.

Reactive power control through SCOSTS objective has one drawback: for the formulation in Table 1, it is hard to find a solution when including PV reactive compensation. For example, for maximum PV integration, including reactive compensation increases simulation time by 22 times (from 11.1 s to 222.1 s without storage and from 20.9 s to 462.9 s with storage). For medium PV integration, the solver is not able to find a solution for the Q DER case within 20 min, while the base case is solved in 11.4 s; now, the medium PV integration with SS case takes almost 2/3 of the time SS-Q DER case requires (form 130.6 s to 209.7 s). For minimum PV integration with storage, including PV reactive compensation almost doubles the simulation time (from

Table 4
Percentage variations due to changes in the circuit model (balanced or unbalanced).

$\Delta_{X,Y}$ are differences between the X and Y circuits, with $X, Y \in \{C, U, B\}$ and C being the CPLT circuit, U being the UNBL circutit and B being the BALN circuit.

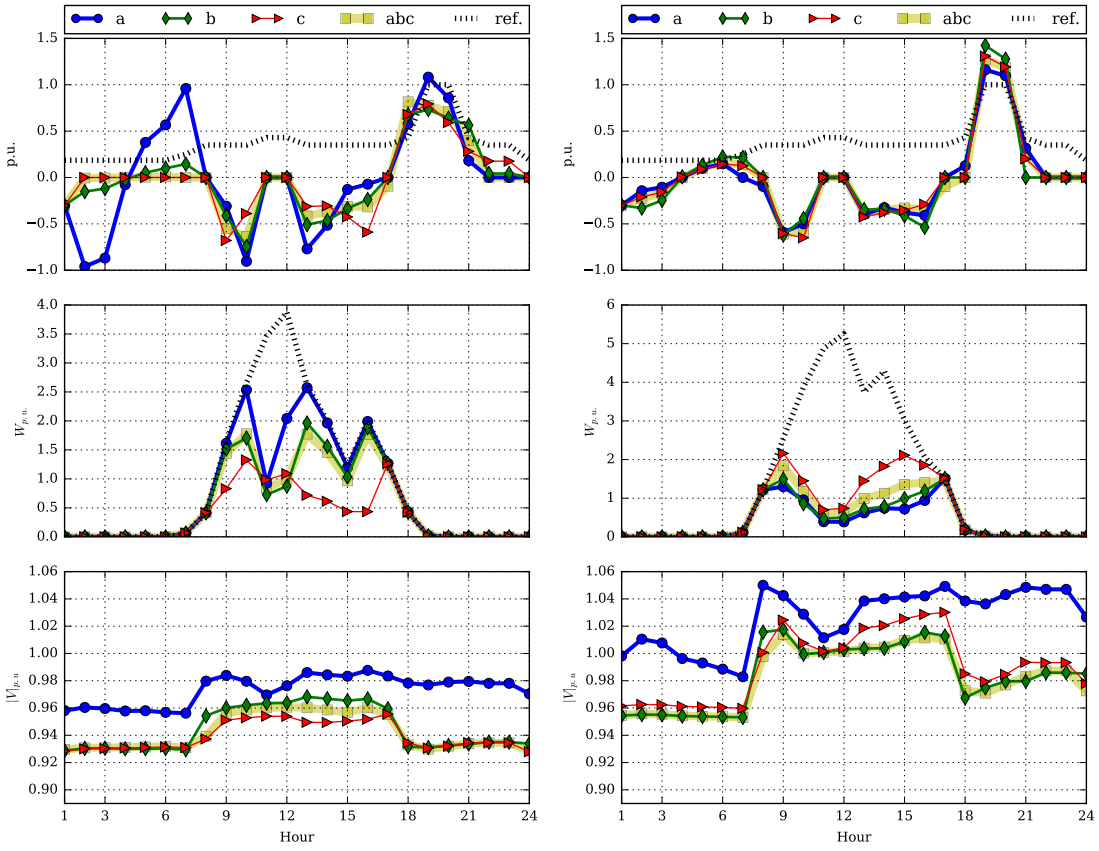

Fig. 2. Comparison between storage active power injections (up, price p.u. as reference), PV system active power injections (middle, total PV available as reference) and voltage profile in time at node 830 (left) and 848 (right), for maximum PV integration and SCOSTS objective.

Table 5
Results between solutions.

	PF	OPF cases				
		No DERs	PCOSTS	SCOSTS	LOSS	SLF-LOSS
f^P	3711.01	3619.58	−735.47	718.801	724.111	723.695
L_T	7.3105	7.2826	10.1539	2.1057	1.8526	1.8543
P_T^h	49.2442	48.2509	1.2196	15.3536	15.6884	15.6593
Q_T^h	17.3669	17.2517	29.6541	5.9153	5.9183	5.9052

f^P in [$], L_T and P_T^h in [MWh] and Q_T^h in [MVArh].

37.2 s to 69.5 s). Additionally, for the UNBL circuit, SCOSTS exceeds the simulation time limits when including reactive compensation for the maximum and medium irradiances.

From Fig. 3, it is clear that LOSS objective can handle very high irradiances without compromising the maximum 2% of VUF for voltage unbalance [45]. Of course, this comes at the cost of curtailing large amounts of PV energy if necessary: With maximum irradiance and SS-Q DER case, PCOSTS objective curtails approximately 1/6 of the available irradiance, while SCOSTS, LOSS and SLF-LOSS objectives curtail half of the available irradiance.

With minimum irradiance all objectives lead to zero curtailment, however, what is presented above is still valid: PCOSTS objective has lower costs with higher losses and unbalances, while LOSS objective has higher costs with lower losses and unbalance. Unbalance on PCOSTS remains too high, this time, due to storage injections.

In conclusion, when renewable energy availability is such that there are no reversed flows, minimizing PCOSTS or LOSS lead to similar results for balanced and unbalanced conditions. For higher integrations, LOSS minimization also minimizes reversed flows (if such flows increase system losses) and increases the PV curtailment. On the other hand, LOSS minimization yields lower voltage unbalance than SLF-LOSS minimization. In contrast, when minimizing PCOSTS, the network will try to export as much energy as possible, which in turn causes system losses and unbalance to increase.

A closer look to the results of each of the objectives tested revealed that minimizing PCOSTS can work as a surrogate for curtailment minimization. Since this objective accounts for the actual power being curtailed and the resulting network losses, it can be useful when deriving locational marginal prices in a distribution network with DERs. However, this objective needs to be handled carefully when dispatching high PV integrations, since the resulting schedule may induce unbalances higher than the recommended minimum for a secure network operation.

Furthermore, when trying to minimize voltage unbalance, the solver often exceeded the maximum simulation time criteria, which makes this approach unreliable for controlling voltage unbalance with the present formulation. Therefore, it is recommended to limit voltage unbalance with inequality constraints.

For high PV integration, losses minimization is better handled by minimizing the SCOSTS or the LOSS objectives. The former is the best option when treating only DERs with PV curtailment, because of its reasonable reactive power control, fast answers and lower active power costs; whereas the latter objective is a better option when including storage and reactive compensation.

It is worth mentioning that for low PV integration, PCOSTS minimization is the best at balancing losses and costs. On the other hand, since SCOSTS minimization have a very poor performance when including reactive power compensation, for high PV integration a combination of PCOSTS and LOSS minimization give a better balance between losses and energy consumption costs at the header.

5.3. DER variations

In Table 6 is summarized the DER impacts for each circuit and selected objectives and parameters, given a maximum and medium irradiance. There, one can observe that DER changes are poorly reflected on the BALN circuit for PCOSTS objective. In contrast, for all other objectives, changes are well estimated.

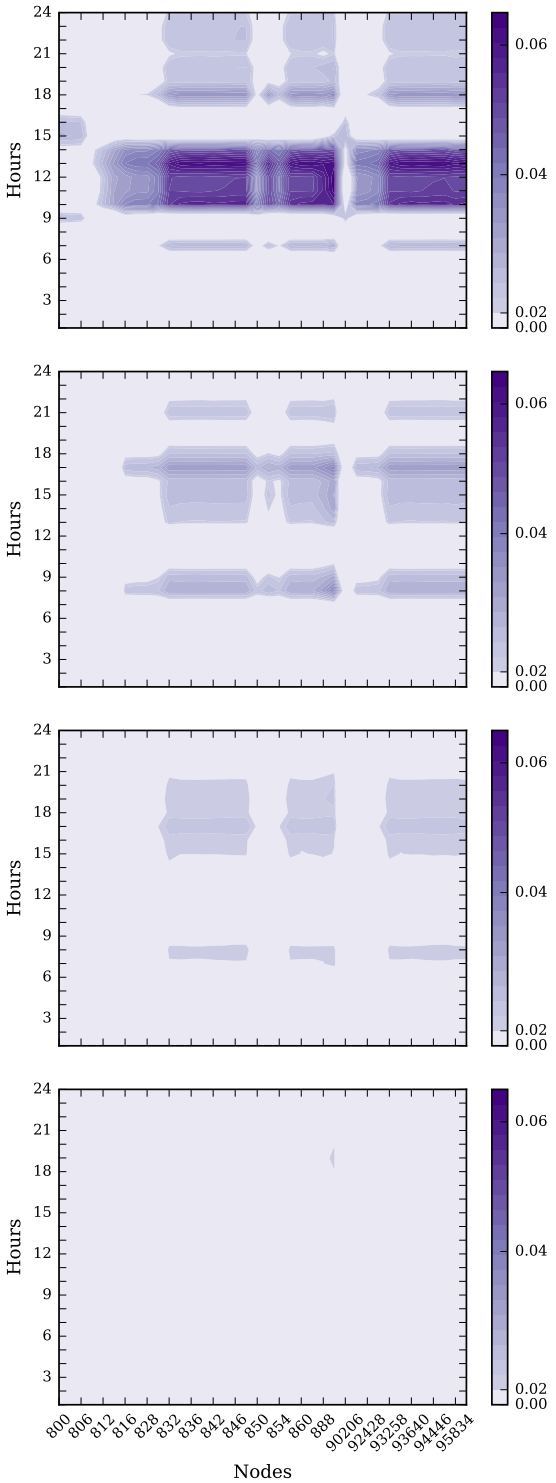

Fig. 3. Negative sequence VUF, for maximum solar irradiance and SS-Q DER case, for each objective, from top to bottom: PCOSTS, SCOSTS, SLF-LOSS and LOSS.

For SCOSTS and LOSS objectives, system storage has more impact on total costs and total curtailed power. For example, Table 6.a (f^P rows, SCOSTS columns) shows that, with or without reactive compensation, including system storage reduces up to 56% of the active power costs at the header; while with or without storage, including reactive compensation only reduces it up to 2.3%.

On the other hand, including reactive power compensation have a major impact on total imported reactive power (see Table 6.a Q_T^h rows, SCOSTS columns), e.g., with or without storage, reactive power injections at the header are reduced by around 60% if PV reactive compensation is enabled.

Looking at Table 6.a (L_T rows, SCOSTS and LOSS columns), one can see that storage and reactive compensation have a similar impact on total system losses by themselves and when combined.

With PCOSTS as objective function, total system losses are 133% higher because of the increase on the reactive power consumption (see Table 6.b, L_T rows, PCOSTS column). Losses change from approximately 4 MWh to 10 MWh, with or without storage, when using reactive compensation.

Reactive power compensation and system storage have the same effect on power injections at the header (see Table 6.b, P_T^h rows, PCOSTS columns). Active power injections at the header go from 9 MWh to 5 MWh when including reactive compensation or storage; and they go from 5 MWh to 1 MWh when both reactive compensation and storage are available. It is also observed that the impact on total imported active power of having both reactive compensation and system storage is almost the sum of the individual impacts.

On the other hand, curtailed PV energy is mainly affected by reactive compensation, but it can be reduced further by having a storage system available (see Table 6.b, p_T rows, PCOSTS columns).

As presented in Table 6.b, for medium PV integration, SCOSTS and LOSS objectives variations on DER are similar to those observed with maximum irradiance. In contrast, reducing PV integration yields a different pattern for PCOSTS objective. Namely, including storage while having reactive compensation presents the bigger change in costs of power injections at the system header; on the other hand, reactive compensation and storage have a similar impact on curtailed PV energy. Furthermore, curtailed energy is zero when both, reactive compensation and storage are available.

Now, when considering unbalanced DER injections, the reduction of system unbalance has little to no effects on the optimal solution. Moreover, it seems impossible to arbitrarily reduce system unbalance with DERs, since there is a minimum feasible unbalance higher than the minimum unbalance achieved without DERs.

Table 6
Percentage variations due to DER changes for maximum (a) and medium (b) PV integration.

(a)

	PCOSTS			SCOSTS			LOSS			
	CPLT	UNBL	BALN	CPLT	UNBL	BALN	CPLT	UNBL	BALN	
Δ(SS)	156.0	156.9	262.4	55.4	55.4	56.2	55.6	55.7	55.6	f^o
Δ(SS-Q)	277.2	279.1	865.6	56.0		56.8	56.4	56.5	56.8	
Δ(Q)	42.7	42.7	69.7	0.9		1.0	1.8	1.9	2.3	
Δ(Q-SS)	-81.5	-80.2	-42.6	2.3	2.3	2.2	3.5	3.5	5.0	
Δ(SS)	-4.1	-4.1	-3.9	19.7	19.8	19.7	20.7	20.8	21.4	L_T
Δ(SS-Q)	-6.1	-6.0	-6.9	26.1		27.7	27.1	27.4	28.4	
Δ(Q)	-129.2	-130.2	-134.3	20.8		23.7	23.0	23.6	24.2	
Δ(Q-SS)	-133.6	-134.3	-127.7	27.1	27.7	31.3	29.2	29.9	30.9	
Δ(SS)	40.0	40.3	62.4	27.8	27.9	28.4	27.2	27.3	26.8	P_T^h
Δ(SS-Q)	76.5	77.2	247.7	28.2		28.7	27.5	27.6	27.4	
Δ(Q)	44.3	44.4	75.1	1.0		1.0	1.7	1.8	2.3	
Δ(Q-SS)	78.2	78.8	197.7	1.5	1.5	1.5	2.2	2.2	3.1	
Δ(SS)	-2.5	-2.5	-3.4	1.5	1.5	1.5	1.5	1.4	1.5	Q_T^h
Δ(SS-Q)	-4.5	-4.4	-4.1	4.3		4.0	4.3	4.5	4.0	
Δ(Q)	-61.1	-59.5	-48.2	61.0		60.8	61.9	61.1	62.5	
Δ(Q-SS)	-64.2	-62.5	-49.3	62.1	61.6	61.8	63.0	62.4	63.4	
Δ(SS)	18.7	18.6	22.9	15.3	15.3	15.3	15.6	15.6	15.9	p_T
Δ(SS-Q)	31.0	30.9	42.8	15.6		15.6	15.6	15.3	15.6	
Δ(Q)	33.1	32.9	43.9	1.4		1.8	0.3	0.4	-2.0	
Δ(Q-SS)	43.3	43.0	58.3	1.8	1.7	2.1	0.3	0.0	-2.4	

(b)

	PCOSTS			SCOSTS			LOSS			
	CPLT	UNBL	BALN	CPLT	UNBL	BALN	CPLT	UNBL	BALN	
Δ(SS)	90.6	90.9	116.1	50.9	50.9	51.4	51.5	51.5	51.8	f^o
Δ(SS-Q)	104.2	104.6	124.7			52.6	51.5	51.5	52.9	
Δ(Q)	16.1	16.1	16.6			1.4	0.6	0.6	1.9	
Δ(Q-SS)	137.7	142.4	-27.7	4.5	2.5	3.8	0.5	0.5	4.2	
Δ(SS)	-9.8	-9.9	-15.7	21.4	21.5	22.2	20.7	20.9	21.5	L_T
Δ(SS-Q)	4.0	3.4	28.1			27.9	25.9	26.2	27.4	
Δ(Q)	-72.5	-73.0	-70.3			22.2	20.1	20.7	21.4	
Δ(Q-SS)	-50.9	-52.1	-5.8	23.6	26.3	27.9	25.3	26.1	27.3	
Δ(SS)	20.3	20.4	22.5	25.3	25.3	25.6	24.9	24.9	24.6	P_T^h
Δ(SS-Q)	20.1	20.2	11.8			26.4	24.6	24.6	25.2	
Δ(Q)	16.0	16.0	16.1			1.5	0.5	0.6	2.0	
Δ(Q-SS)	15.8	15.9	4.5	1.3	1.7	2.6	0.2	0.2	2.8	
Δ(SS)	-3.5	-3.4	-4.1	1.5	1.4	1.5	1.6	1.5	1.7	Q_T^h
Δ(SS-Q)	-1.6	-2.1	22.4			3.9	3.9	4.1	3.9	
Δ(Q)	-32.7	-31.7	-15.7			57.2	57.5	56.6	58.6	
Δ(Q-SS)	-30.3	-29.9	13.7	58.0	57.8	58.2	58.5	57.8	59.6	
Δ(SS)	55.5	55.3	86.1	36.4	36.3	35.8	37.3	37.2	39.1	p_T
Δ(SS-Q)	100.0	100.0	100.0			37.2	36.6	36.4	37.7	
Δ(Q)	58.2	57.9	85.7			4.5	-1.0	-1.0	-4.4	
Δ(Q-SS)	100.0	100.0	100.0	5.7	6.4	6.5	-2.3	-2.3	-6.8	

6. Conclusions

This paper presented a comprehensive study on the errors induced by assuming balanced conditions in modern distribution networks. We demonstrated with the different case studies implemented that it is necessary to solve a 3ϕ-ACOPF, not only to schedule DERs properly in an unbalanced distribution system but to understand and provide better solutions.

For example, in Section 5.1, we showed that when the objective function causes a reduction in system unbalance (e.g., active power losses minimization), the errors between unbalanced and balanced circuits are low. Moreover, as presented in Section 5.3 changes in available DERs in the system can be predicted using the single-line equivalent under these induced balanced conditions. This comes at the cost of reducing the hosting capacity of the network, i.e., all additional PV energy available beyond a point is curtailed to maintain such balanced conditions. Therefore, there is a trade-off between the network hosting capacity and the network unbalance.

With the above in mind, the conditions for using a single-line equivalent to model an unbalance power distribution network with DERs can be summarized in the following two guidelines: (1) Check if the optimal operation point induce a low voltage unbalance. For example, since the lowest network losses are those appearing without unbalance, minimizing the losses in an unbalanced network would yield a low unbalance overall; or, (2) Check if the integration of renewable energy is low enough. For example, when maximizing active power exports, if the renewable energy integration is such that creates a significant amount of reversed flows (i.e., power flowing from the feeder to the header) you could expect an increase in voltage unbalance. Therefore, if the reversed flows are low enough, network unbalance will not increase when maximizing power exports. Thus, after checking if any of these two guidelines are valid, and if the resulting unbalance is low enough, a single-line equivalent could give a good initial estimate of the network state for an unbalanced network or may be used as a way to improve the performance of 3ϕ-ACOPF, e.g., for a warm start. Note that this is a crucial property to save computation time as the size and complexity of the network being analyzed increase.

Leaving aside the impact on network unbalance, and as presented in Section 5.3, under unbalanced conditions, for maximum irradiance, and while minimizing active power import costs, reactive compensation behaves as expected by having more impact on power curtailment. In contrast, reactive compensation and storage have the same impact for medium irradiance. Whatever the case, having both yields lower curtailment among all cases.

Simulations results presented in Section 5.3 also showed that storage significantly impacts active power costs and curtailed energy for weighted squared apparent power import costs or full-losses minimization. On the other hand, reactive power compensation and storage have the same impact on system losses. The latter is also true for all objectives when considering minimum PV integration, being the impact of storage more relevant when minimizing active power import costs.

In this paper we rise the awareness about the error of single-line equivalents for modern distribution systems; it is therefore worthwhile for researchers to check for their specific cases if this error is acceptable or not, which could change by the system network size and integration levels of variable renewable energy and/or DER. As a future work we propose to verify the results in other networks and objectives, test other solution methods and algorithms performance, and find formal guarantees for the solutions here presented. Steps further away in this line of research are: (1) Application of sensitivity analysis of the presented formulation to design network-aware local control strategies for DERs and derive active and reactive power pricing schemes; (2) Analysis of long/medium term congestion management in distribution networks with DER planning by including integer variables in the presented model; (3) Comparative study of the presented formulation and its Mixed-Integer Programming alternative to control the storage systems.

CRediT authorship contribution statement

I.D. Serna-Suárez: Conceptualization, Writing – original draft, Methodology, Formal analysis, Investigation, Visualization, Software. **G. Morales-España:** Methodology, Writing – review & editing. **M. de Weerdt:** Methodology, Writing – review & editing. **G. Carrillo-Caicedo:** Supervision, Validation, Resources, Writing – review & editing. **G. Ordóñez-Plata:** Supervision, Validation, Resources. **O.A. Quiroga:** Writing – review & editing, Funding acquisition.

Declaration of competing interest

The authors declare that they have no known competing financial interests or personal relationships that could have appeared to influence the work reported in this paper.

Data availability

Data will be made available on request.

References

[1] I.E. Agency, Renewables 2022, Technical Report, IEA, 2022, URL https://www.iea.org/reports/renewables-2022.

[2] I.E. Agency, Global EV Outlook 2022, Technical Report, IEA, 2022, URL https://www.iea.org/reports/global-ev-outlook-2022.

[3] M. Chamana, B.H. Chowdhury, F. Jahanbakhsh, Distributed control of voltage regulating devices in the presence of high PV penetration to mitigate ramp-rate issues, IEEE Trans. Smart Grid 9 (2018) 1086–1095, http://dx.doi.org/10.1109/TSG.2016.2576405.

[4] H. Mortazavi, H. Mehrjerdi, M. Saad, S. Lefebvre, D. Asber, L. Lenoir, A monitoring technique for reversed power flow detection with high PV penetration level, IEEE Trans. Smart Grid 6 (2015) 2221–2232, http://dx.doi.org/10.1109/TSG.2015.2397887.

[5] V.H.M. Quezada, J.R. Abbad, T.G.S. Roman, Assessment of energy distribution losses for increasing penetration of distributed generation, IEEE Trans. Power Syst. 21 (2006) 533–540, http://dx.doi.org/10.1109/TPWRS.2006.873115.

[6] H.A. Gil, G. Joos, Models for quantifying the economic benefits of distributed generation, IEEE Trans. Power Syst. 23 (2008) 327–335, http://dx.doi.org/10.1109/TPWRS.2008.920718.

[7] W.G.C. 6.19, Planning and Optimization Methods for Active Distribution Systems, Technical Report, CIGRE, 2014, URL https://e-cigre.org/publication/591-planning-and-optimization-methods-for-distribution-systems.

[8] W.G.C. 6.11, Development and Operation of Active Distribution Networks, Technical Report, CIGRE, 2011, URL https://e-cigre.org/publication/ELT_255_6-development-and-operation-of-active-distribution-networks.

[9] S. Bahramirad, A. Khodaei, R. Masiello, Distribution markets, IEEE Power Energy Mag. 14 (2016) 102–106, http://dx.doi.org/10.1109/MPE.2016.2543121.

[10] A.K. Erenoğlu, İbrahim Şengör, O. Erdinç, A. Taşcıkaraoğlu, J.P. Catalão, Optimal energy management system for microgrids considering energy storage, demand response and renewable power generation, Int. J. Electr. Power Energy Syst. 136 (2022) 107714, http://dx.doi.org/10.1016/j.ijepes.2021.107714.

[11] S. Vonsien, R. Madlener, Li-ion battery storage in private households with PV systems: Analyzing the economic impacts of battery aging and pooling, J. Energy Storage 29 (2020) http://dx.doi.org/10.1016/j.est.2020.101407.

[12] T. Zhang, W. Qiu, Z. Zhang, Z. Lin, Y. Ding, Y. Wang, L. Wang, L. Yang, Optimal bidding strategy and profit allocation method for shared energy storage-assisted VPP in joint energy and regulation markets, Appl. Energy 329 (2023) http://dx.doi.org/10.1016/j.apenergy.2022.120158.

[13] Z. Wang, C. Gu, F. Li, Flexible operation of shared energy storage at households to facilitate PV penetration, Renew. Energy 116 (2018) 438–446, http://dx.doi.org/10.1016/j.renene.2017.10.005.

[14] W.G.C. 6.24, Capacity of Distribution Feeders for Hosting DER, Technical Report, CIGRE, 2014, URL https://e-cigre.org/publication/ELT_255_6-development-and-operation-of-active-distribution-networks.

[15] K. Girigoudar, L.A. Roald, On the impact of different voltage unbalance metrics in distribution system optimization, Electr. Power Syst. Res. 189 (2020) http://dx.doi.org/10.1016/j.epsr.2020.106656.

[16] J. Baran, A.R., T. Fernandes, A three-phase optimal power flow applied to the planning of unbalanced distribution networks, Int. J. Electr. Power Energy Syst. 74 (2016) 301–309, http://dx.doi.org/10.1016/j.ijepes.2015.07.004.

[17] S. Dahal, H. Salehfar, Impact of distributed generators in the power loss and voltage profile of three phase unbalanced distribution network, Int. J. Electr. Power Energy Syst. 77 (2016) 256–262, http://dx.doi.org/10.1016/j.ijepes.2015.11.038.

[18] P. De Oliveira-De Jesus, C. Henggeler Antunes, A detailed network model for distribution systems with high penetration of renewable generation sources, Electr. Power Syst. Res. 161 (2018) 152–166, http://dx.doi.org/10.1016/j.epsr.2018.04.005.

[19] H. Ahmadi, J.R. Martí, A. von Meier, A linear power flow formulation for three-phase distribution systems, IEEE Trans. Power Syst. 31 (2016) 5012–5021, http://dx.doi.org/10.1109/TPWRS.2016.2533540.

[20] J.S. Giraldo, P.P. Vergara, J.C. López, P.H. Nguyen, N.G. Paterakis, A linear AC-OPF formulation for unbalanced distribution networks, IEEE Trans. Ind. Appl. 57 (2021) 4462–4472, http://dx.doi.org/10.1109/TIA.2021.3085799.

[21] A. Heidari-Akhijahani, A. Safdarian, M. Vrakopoulou, A linear AC power flow model for unbalanced multi-phase distribution networks based on current injection equations, IEEE Trans. Power Syst. 36 (2021) 3806–3809, http://dx.doi.org/10.1109/TPWRS.2021.3073839.

[22] A. Garces, A quadratic approximation for the optimal power flow in power distribution systems, Electr. Power Syst. Res. 130 (2016) 222–229, http://dx.doi.org/10.1016/j.epsr.2015.09.006.

[23] M. Cai, R. Yang, Y. Zhang, Iteration-based linearized distribution-level locational marginal price for three-phase unbalanced distribution systems, IEEE Trans. Smart Grid 12 (2021) 4886–4896, http://dx.doi.org/10.1109/TSG.2021.3094494.

[24] R.R. Jha, A. Dubey, Network-level optimization for unbalanced power distribution system: Approximation and relaxation, IEEE Trans. Power Syst. 36 (2021) 4126–4139, http://dx.doi.org/10.1109/TPWRS.2021.3066146.

[25] I.D. Serna-Suárez, G. Carrillo-Caicedo, G.A. Morales-España, M. De Weerdt, G. Ordóñez Plata, A convex approximation for optimal DER scheduling on unbalanced power distribution networks, Dyna (2019) http://dx.doi.org/10.15446/dyna.v86n208.72886.

[26] E. Stai, C. Wang, J.-Y. Le Boudec, On the solution of the optimal power flow for three-phase radial distribution networks with energy storage, IEEE Trans. Control Netw. Syst. 8 (2021) 187–199, http://dx.doi.org/10.1109/TCNS.2020.3024319.

[27] W. Huang, W. Zheng, D.J. Hill, Distributionally robust optimal power flow in multi-microgrids with decomposition and guaranteed convergence, IEEE Trans. Smart Grid 12 (2021) 43–55, http://dx.doi.org/10.1109/TSG.2020.3012025.

[28] R. Hu, Q. Li, F. Qiu, Ensemble learning based convex approximation of three-phase power flow, IEEE Trans. Power Syst. 36 (2021) 4042–4051, http://dx.doi.org/10.1109/TPWRS.2021.3055481.

[29] S. Karagiannopoulos, P. Aristidou, G. Hug, Data-driven local control design for active distribution grids using off-line optimal power flow and machine learning techniques, IEEE Trans. Smart Grid 10 (2019) 6461–6471, http://dx.doi.org/10.1109/TSG.2019.2905348.

[30] E. Mulenga, M.H.J. Bollen, N. Etherden, A review of hosting capacity quantification methods for photovoltaics in low-voltage distribution grids, Int. J. Electr. Power Energy Syst. 115 (2020) 105445, http://dx.doi.org/10.1016/j.ijepes.2019.105445.

[31] B.A. Robbins, A.D. Domínguez-García, Optimal reactive power dispatch for voltage regulation in unbalanced distribution systems, IEEE Trans. Power Syst. 31 (2016) 2903–2913, http://dx.doi.org/10.1109/TPWRS.2015.2451519.

[32] P. Li, H. Ji, C. Wang, J. Zhao, G. Song, F. Ding, J. Wu, Optimal operation of soft open points in active distribution networks under three-phase unbalanced conditions, IEEE Trans. Smart Grid PP (2017) 1, http://dx.doi.org/10.1109/TSG.2017.2739999.

[33] A.S. Zamzam, N.D. Sidiropoulos, E. Dall'Anese, Beyond relaxation and Newton-Raphson: Solving AC OPF for multi-phase systems with renewables, IEEE Trans. Smart Grid PP (2017) 1, http://dx.doi.org/10.1109/TSG.2016.2645220.

[34] G. Carpinelli, F. Mottola, D. Proto, P. Varilone, Minimizing unbalances in low-voltage microgrids: Optimal scheduling of distributed resources, Appl. Energy 191 (2017) 170–182, http://dx.doi.org/10.1016/j.apenergy.2017.01.057.

[35] P.A.N. Garcia, J.L.R. Pereira, S. Carneiro, V.M. da Costa, N. Martins, Three-phase power flow calculations using the current injection method, IEEE Trans. Power Syst. 15 (2000) 508–514, http://dx.doi.org/10.1109/59.867133.

[36] D.R.R. Penido, L.R. de Araujo, S. Carneiro, J.L.R. Pereira, P.A.N. Garcia, Three-phase power flow based on four-conductor current injection method for unbalanced distribution networks, IEEE Trans. Power Syst. 23 (2008) 494–503, http://dx.doi.org/10.1109/TPWRS.2008.919423.

[37] L.R. Araujo, D.R.R. Penido, S. Carneiro, J.L.R. Pereira, A three-phase optimal power-flow algorithm to mitigate voltage unbalance, IEEE Trans. Power Deliv. 28 (2013) 2394–2402, http://dx.doi.org/10.1109/TPWRD.2013.2261095.

[38] J.F. Franco, M.J. Rider, R. Romero, A mixed-integer linear programming model for the electric vehicle charging coordination problem in unbalanced electrical distribution systems, IEEE Trans. Smart Grid 6 (2015) 2200–2210, http://dx.doi.org/10.1109/TSG.2015.2394489.

[39] F. Meng, B. Chowdhury, M. Chamana, Three-phase optimal power flow for market-based control and optimization of distributed generations, IEEE Trans. Smart Grid PP (2017) 1, http://dx.doi.org/10.1109/TSG.2016.2638963.

[40] R. Madani, S. Sojoudi, J. Lavaei, Convex relaxation for optimal power flow problem: Mesh networks, IEEE Trans. Power Syst. 30 (2015) 199–211, http://dx.doi.org/10.1109/TPWRS.2014.2322051.

[41] J.D. Watson, N.R. Watson, I. Lestas, Optimized dispatch of energy storage systems in unbalanced distribution networks, IEEE Trans. Sustain. Energy PP (2017) 1, http://dx.doi.org/10.1109/TSTE.2017.2752964.

[42] X. Su, M.A.S. Masoum, P.J. Wolfs, Optimal PV inverter reactive power control and real power curtailment to improve performance of unbalanced four-wire LV distribution networks, IEEE Trans. Sustain. Energy 5 (2014) 967–977, http://dx.doi.org/10.1109/TSTE.2014.2313862.

[43] S. Gill, I. Kockar, G.W. Ault, Dynamic optimal power flow for active distribution networks, IEEE Trans. Power Syst. 29 (2014) 121–131, http://dx.doi.org/10.1109/TPWRS.2013.2279263.

[44] W.H. Kersting, Radial distribution test feeders, in: 2001 IEEE Power Engineering Society Winter Meeting. Conference Proceedings (Cat. No.01CH37194), volume 2, 2001, pp. 908–912, http://dx.doi.org/10.1109/PESW.2001.916993.

[45] IEC, Testing and Measurement Techniques-Power Quality Measurement Methods, Technical Report IEC 61000.4.30: Electromagnetic compatibility (EMC) Part4.30, 2015, URL https://webstore.iec.ch/publication/68642.